

**Highly efficient nuclear excitation via highly nonlinear light-nucleus interaction**Hanxu Zhang <sup>1</sup>, Tao Li <sup>1</sup> and Xu Wang <sup>1,2,\*</sup><sup>1</sup>Graduate School, China Academy of Engineering Physics, Beijing 100193, China<sup>2</sup>Southern Center for Nuclear-Science Theory, Institute of Modern Physics, Chinese Academy of Sciences, Huizhou, Guangdong 516000, China

(Received 30 December 2024; accepted 7 April 2025; published 30 April 2025)

In our recent publication [H. Zhang, T. Li, and X. Wang, *Phys. Rev. Lett.* **133**, 152503 (2024)], we demonstrate that the interaction between hydrogenlike thorium-229 ions ( $^{229}\text{Th}^{89+}$ ) and contemporary intense lasers can access a highly nonlinear and nonperturbative regime of light-nucleus interaction. This interaction enables highly efficient nuclear isomeric excitation of  $^{229}\text{Th}$ , achieving an excitation probability exceeding 10% per nucleus per femtosecond laser pulse. In this paper, we significantly expand on our previous work by providing a detailed theoretical framework, extended numerical results, and comprehensive analysis. We emphasize that the role of the electron is crucial in enhancing light-nucleus interactions, particularly through a nuclear hyperfine mixing effect. We also show that the nuclear isomeric excitation can be further optimized to approximately 90% per nucleus per pulse.

DOI: [10.1103/PhysRevC.111.044614](https://doi.org/10.1103/PhysRevC.111.044614)**I. INTRODUCTION**

Efficient excitation of atomic nuclei holds significant promise for advanced nucleus-based applications, including nuclear clocks [1–4], nuclear lasers [5–7], nuclear isomer batteries [8,9], etc. A variety of methods for nuclear excitation have been explored, such as optical excitation [10–16], Coulomb excitation [17–20], electronic excitation [21–24], and hybrid optical-electronic excitation techniques [25–32]. However, nearly all existing nuclear excitation methods operate within the linear, perturbative regime. In this regime, the excitation probability of an individual nucleus is typically very low, necessitating the presence of large numbers of nuclei to detect nuclear excitation signals.

Nonlinear nuclear excitation, on the other hand, could substantially increase the single-nucleus excitation probability. Over the past few decades, intense lasers have been demonstrated to induce highly nonlinear responses in atoms, leading to efficient atomic excitation, ionization, and control [33–35]. For instance, a single femtosecond laser pulse can remove several or even dozens of electrons from a single atom [36]. Achieving similar control over atomic nuclei could bring us closer to realizing advanced nucleus-based technologies. However, initiating nonlinear responses in nuclei has proven exceptionally difficult, mainly due to the small nuclear transition moments, which limit the coupling strength between the nucleus and external laser fields. As a result, the energy of the laser-nucleus coupling is typically much smaller than the nuclear transition energy, rendering it a weak perturbation.

Recently, we identified an exception to this limitation. We predicted that the interaction between hydrogenlike thorium-229 ions ( $^{229}\text{Th}^{89+}$ ) and currently available intense laser fields

could enable a highly nonlinear and nonperturbative regime of light-nucleus interaction [37]. This possibility hinges on three key elements: (a) the existence of a low-lying excited state in the  $^{229}\text{Th}$  nucleus, with an energy of only 8.36 eV above the ground state [2–4,38]; (b) a nuclear hyperfine mixing (NHM) effect that significantly enhances the light-nucleus coupling strength; and (c) the high intensities achievable with modern laser systems, with recent records reaching  $10^{23}$  W/cm<sup>2</sup> [39,40]. The resulting highly nonlinear light-nucleus interaction is predicted to enable highly efficient nuclear isomeric excitation, with probabilities greater than 10% per nucleus per femtosecond laser pulse [37]. Additionally, the laser-driven  $^{229}\text{Th}^{89+}$  system generates secondary radiation in the form of high-order harmonics of the driving laser.

The goal of the current article is to expand upon our previous Letter [37] by presenting a more detailed theoretical framework, extended numerical results, and comprehensive analyses. Specifically, we provide an in-depth derivation of the NHM effect and the light-nucleus interaction, introducing a transition moment that accounts for hyperfine mixing. Our approach highlights the crucial role of the electron in radiative transitions and establishes a direct connection between these transitions and laser-excitation processes. Through numerical analysis, we demonstrate the breakdown of perturbation theory and emphasize the highly nonlinear effects. The nuclear isomeric excitation probability is further optimized, reaching over 90% per nucleus per laser pulse. We also investigate the impact of laser duration and the dynamics of the  $1s$  electron, confirming the robustness of our approach.

The article is organized as follows. Section II provides a detailed explanation of the NHM effect and light-nucleus interaction. Section III presents numerical results, including nuclear excitation and population dynamics for both bare nuclei and hydrogenlike ions, as well as an analysis of how the  $1s$  electron enhances the light-nucleus interaction. Section IV

\*Contact author: [xwang@giscaep.ac.cn](mailto:xwang@giscaep.ac.cn)

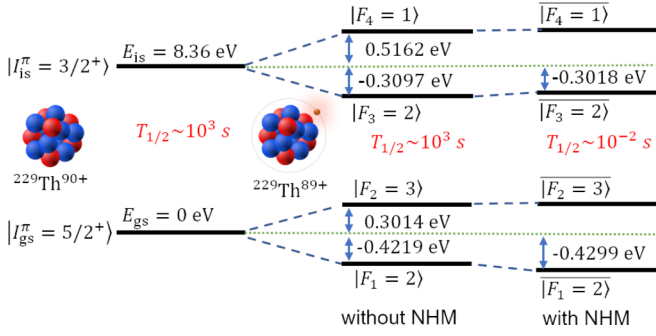


FIG. 1. Energy level diagrams of the  $^{229}\text{Th}$  ion. Left: Ground state and isomeric state of the bare nucleus ( $^{229}\text{Th}^{90+}$ ). Center: Hyperfine energy levels of the hydrogenlike ion ( $^{229}\text{Th}^{89+}$ ) without the NHM effect. Right: Hyperfine energy levels with the NHM effect included. Note that the energy splittings are not drawn to scale, and the radiative half-life for each case is indicated in red.

includes further discussions and remarks, and the conclusion is presented in Sec. V.

## II. METHODS

### A. Energy structures of $^{229}\text{Th}^{90+}$ and $^{229}\text{Th}^{89+}$

Figure 1 illustrates the energy structures of  $^{229}\text{Th}^{90+}$  and  $^{229}\text{Th}^{89+}$ . For the bare nucleus,  $^{229}\text{Th}^{90+}$ , the energy of the isomeric state lies approximately 8.36 eV above the ground state [2–4]. The ground state has spin-parity  $I_{\text{gs}}^{\pi} = 5/2^{+}$ , while the isomeric state has  $I_{\text{is}}^{\pi} = 3/2^{+}$ . The energy structure is shown in the left part of Fig. 1.

For the  $^{229}\text{Th}^{89+}$  ion, a  $1s$  electron with angular momentum  $J = 1/2$  couples to the nucleus, leading to a splitting of the nuclear ground state into  $|F_1 = 2, m_1\rangle$  and  $|F_2 = 3, m_2\rangle$  states, and a splitting of the isomeric state into  $|F_3 = 2, m_3\rangle$  and  $|F_4 = 1, m_4\rangle$  states. These states are expressed as

$$|F_n, m_n\rangle = \sum_{m_n, m_J} C_{J, m_J, I_n, m_n}^{F_n, m_n} |J, m_J\rangle \otimes |I_n, m_n\rangle, \quad (1)$$

where  $C_{J, m_J, I_n, m_n}^{F_n, m_n}$  is a Clebsch-Gordan coefficient. To simplify notation, the  $n$  index is used collectively to encapsulate information about  $I$ :

$$\begin{aligned} I_n &= I_{\text{gs}} & \text{if } n &= 1, 2, \\ I_n &= I_{\text{is}} & \text{if } n &= 3, 4. \end{aligned}$$

This electron-nucleus system is governed by the Hamiltonian  $H_0 = H_e + H_n + V_{\text{HF}}$ , where  $H_e$  and  $H_n$  represent the Hamiltonians for the electron and the nucleus, respectively, and  $V_{\text{HF}}$  is the hyperfine interaction between them [41]:

$$V_{\text{HF}} = \sum_{\tau=E, M} \sum_{\lambda\mu} \frac{4\pi}{2\lambda+1} (-1)^{\mu} \mathcal{M}_n^{(\tau\lambda-\mu)} \cdot \mathcal{N}_e^{(\tau\lambda\mu)}, \quad (2)$$

where  $\mathcal{M}_n^{(\tau\lambda\mu)}$  acting in the nuclear subspace is the multipole moment operator of type  $\tau$  ( $E$  for electric,  $M$  for magnetic) and rank  $\lambda$ .  $\mathcal{N}_e^{(\tau\lambda\mu)}$  acting in the electronic subspace is the

multipole transition operator. They can be written as

$$\mathcal{M}_n^{(E\lambda\mu)} = \int \rho_n r^{\lambda} Y_{\lambda\mu}(\theta, \phi) d\tau, \quad (3)$$

$$\mathcal{M}_n^{(M\lambda\mu)} = -\frac{i}{c(\lambda+1)} \int \mathbf{j}_n \cdot \mathbf{L} [r^{\lambda} Y_{\lambda\mu}(\theta, \phi)] d\tau, \quad (4)$$

$$\mathcal{N}_e^{(E\lambda\mu)} = \int \frac{\rho_e}{r^{\lambda+1}} Y_{\lambda\mu}(\theta, \phi) d\tau, \quad (5)$$

$$\mathcal{N}_e^{(M\lambda\mu)} = \frac{i}{c\lambda} \int \frac{\mathbf{j}_e \cdot \mathbf{L} [Y_{\lambda\mu}(\theta, \phi)]}{r^{\lambda+1}} d\tau. \quad (6)$$

Here,  $\rho$ ,  $\mathbf{j}$ , and  $\mathbf{L}$  denote the charge density operator, current density operator, and angular momentum operator, respectively.  $Y_{\lambda\mu}$  is spherical harmonics.

Using Eqs. (1)–(6), the energy splitting of each  $F$  state can be determined from the matrix elements of  $V_{\text{HF}}$

$$\begin{aligned} &\langle F_m, m_m | V_{\text{HF}} | F_n, m_n \rangle \\ &= \delta_{F_n m_n, F_m m_m} (-1)^{J+I_n+F_m} \sum_{\tau\lambda} \frac{4\pi}{2\lambda+1} \mathcal{M}_{I_n I_n}^{(\tau\lambda)} \mathcal{N}_{JJ}^{(\tau\lambda)} \\ &\quad \times W(J, I_m, J, I_n; F_m, \lambda), \end{aligned} \quad (7)$$

where  $\mathcal{M}_{I_n I_n}^{(\tau\lambda)} \equiv \langle I_n || \mathcal{M}_n^{(\tau\lambda)} || I_n \rangle$  and  $\mathcal{N}_{JJ}^{(\tau\lambda)} \equiv \langle J || \mathcal{N}_e^{(\tau\lambda)} || J \rangle$  are reduced matrix elements.  $W$  is the Racah-Wigner coefficient. The electronic matrix element is evaluated using the Wigner-Eckart theorem and numerical calculation of electron wave function [42].

Diagonal nuclear matrix elements are determined by relating them to established nuclear multipole moments (Eqs. 3–40 in [43]). For example, the magnetic dipole moment is given by

$$\mu_I = \sqrt{\frac{4\pi}{3(2I+1)}} C_{I, I, 1, 0}^{I, I} \mathcal{M}_I^{(M1)}. \quad (8)$$

The experimentally measured nuclear magnetic moments are  $\mu_{I_{\text{gs}}} = 0.36\mu_N$  and  $\mu_{I_{\text{is}}} = -0.37\mu_N$  [44,45], with  $\mu_N$  being the nuclear magneton. The diagonal matrix elements correspond to the hyperfine splitting energies. The calculated hyperfine energy structure, neglecting magnetic quantum numbers due to degeneracy, is presented in the central part of Fig. 1.

Beyond the standard hyperfine structure, state mixing between  $F$  states with different  $I$  can occur, referred to as the NHM effect [46–49]. This mixing arises from the nonzero off-diagonal matrix elements of  $V_{\text{HF}}$ . In the  $^{229}\text{Th}^{89+}$  system,  $|F_1 = 2, m_1\rangle$  and  $|F_3 = 2, m_3\rangle$  states correspond to different nuclear states. When these states share the same magnetic quantum number ( $m_1 = m_3 = m$ ), the matrix element  $\langle F_1, m | V_{\text{HF}} | F_3, m \rangle$  can be nonzero.

The off-diagonal nuclear reduced matrix elements can be expressed in terms of the reduced transition probability as

$$B(\tau\lambda; I_n \rightarrow I_m) \equiv \frac{|\mathcal{M}_{I_n I_n}^{(\tau\lambda)}|^2}{2I_n + 1}. \quad (9)$$

State mixing is incorporated by diagonalizing the  $H_0$  matrix, producing the eigenstates of the system. These eigenstates,

denoted with an overline, are expressed as

$$\overline{|F_n, m\rangle} = \sum_m D_{nm} |F_m, m\rangle, \quad (10)$$

where  $D$  is a coefficient matrix:

$$D = \begin{pmatrix} \sqrt{1-b^2} & 0 & -b & 0 \\ 0 & 1 & 0 & 0 \\ b & 0 & \sqrt{1-b^2} & 0 \\ 0 & 0 & 0 & 1 \end{pmatrix}. \quad (11)$$

For  $^{229}\text{Th}^{89+}$ , the mixing coefficient  $b$  is calculated to be  $-0.031$ . Hyperfine structure with the NHM effect included is shown in the right part of Fig. 1.

As shown in Fig. 1, the NHM effect manifests in two primary aspects: (i) a small modification of the energy levels, and (ii) a significant reduction in the radiative half-life of the nuclear excited state, with the possibility of a decrease spanning several orders of magnitude.

Assuming a transition energy  $\Delta E$ , averaging over initial states and summing over final states, the radiative transition rate (of type  $\tau\lambda$ ) for a bare nucleus from  $|I_n\rangle$  to  $|I_m\rangle$  is given by [50]

$$\Gamma_{mn}^b = \frac{8\pi(\lambda+1)}{\lambda[(2\lambda+1)]!!^2} \left(\frac{\Delta E}{\hbar c}\right)^{2\lambda+1} B(\tau\lambda; I_n \rightarrow I_m). \quad (12)$$

For the  $^{229}\text{Th}^{89+}$  system with the NHM effect included, the radiative transition rate from  $\overline{|F_n\rangle}$  to  $\overline{|F_m\rangle}$  is

$$\Gamma_{mn}^{\text{NHM}} = \frac{8\pi(\lambda+1)}{\lambda[(2\lambda+1)]!!^2} \left(\frac{\Delta E}{\hbar c}\right)^{2\lambda+1} |\mathcal{M}(\tau\lambda; \overline{F_n} \rightarrow \overline{F_m})|^2, \quad (13)$$

where  $\mathcal{M}$  is defined as the reduced multipole transition moment under mixed  $F$  state basis

$$\begin{aligned} \mathcal{M}(\tau\lambda; \overline{F_n} \rightarrow \overline{F_m}) &= \frac{\langle \overline{F_m} | \mathcal{M}_n^{(\tau\lambda)} + \mathcal{M}_e^{(\tau\lambda)} | \overline{F_n} \rangle}{\sqrt{2F_n+1}} \\ &= \sqrt{2F_m+1} \sum_{kh} D_{nk} D_{mh} (-1)^{I_k+I_h} \\ &\quad \times [\delta_{I_k, I_h} \mathcal{M}_{JJ}^{(\tau\lambda)} W(F_n, \lambda, I_h, J; F_m, J) \\ &\quad + (-1)^{F_n+F_m} \mathcal{M}_{I_h I_k}^{(\tau\lambda)} W(F_n, \lambda, J, I_h; F_m, I_k)]. \end{aligned} \quad (14)$$

Here,  $\mathcal{M}_e^{(\tau\lambda)}$  involves replacing the nuclear charge density and current density in Eqs. (3) and (4) with those of the electron.

A comparison between Eqs. (12) and (13) reveals the intrinsic reason of the accelerated  $\gamma$  decay. The presence of the electron introduces a term  $\mathcal{M}_{JJ}^{(\tau\lambda)}$ , which greatly enhances the transition moment. A detailed discussion is provided in Sec. III.

Table I presents the calculated radiative transitions for the excited states of  $^{229}\text{Th}^{90+}$  and  $^{229}\text{Th}^{89+}$ . For the nuclear reduced transition probability, we adopt the value  $B(M1; I_{is} \rightarrow I_{gs}) = 0.008 \text{ W.u.}$ , as calculated by Minkov and Pálffy [51]. The results reveal a remarkable acceleration of the radiative decay by 4–5 orders of magnitude due to the presence of the  $1s$  electron, reducing the half-life from  $\sim 10^3 \text{ s}$  to 10 ms. It is worth noting that the experimentally measured half-life of the isomeric state ranges from 1400 to 2500 s, in isolated triply

TABLE I. Radiative transitions in  $^{229}\text{Th}^{90+}$  and  $^{229}\text{Th}^{89+}$ . For  $^{229}\text{Th}^{89+}$ , the NHM effect is included and  $T_{1/2}$  is the half-life of the initial state.

	Initial state	Final state	$\Gamma \text{ (s}^{-1}\text{)}$	$T_{1/2}$
$^{229}\text{Th}^{90+}$	$ I_{is}^\pi\rangle$	$ I_{gs}^\pi\rangle$	$1.48 \times 10^{-4}$	4697 s
$^{229}\text{Th}^{89+}$	$\overline{ F_4\rangle}$	$\overline{ F_3\rangle}$	13.54	21.48 ms
		$\overline{ F_1\rangle}$	18.73	
	$\overline{ F_3\rangle}$	$\overline{ F_2\rangle}$	10.12	20.52 ms
		$\overline{ F_1\rangle}$	23.66	
	$\overline{ F_2\rangle}$	$\overline{ F_1\rangle}$	6.44	107.52 ms

charged ions [52], or in crystal environments with results adjusted for the free-space situation [2–4, 53]. A discrepancy of 2–3 times between the theoretical  $B(M1)$  value and the experimental measurements is observed. However, this discrepancy does not affect the discussions and conclusions in this article.

## B. Time evolution in a strong laser field

Considering the interaction between a strong laser field and either  $^{229}\text{Th}^{90+}$  or  $^{229}\text{Th}^{89+}$ , the state of the system is governed by a time-dependent Schrödinger equation (TDSE):

$$i\hbar \frac{\partial}{\partial t} |\Psi(t)\rangle = [H_0 + H_I(t)] |\Psi(t)\rangle, \quad (15)$$

where  $H_0$  has been defined above and its eigenstates are given by Eq. (10).  $H_I(t)$  is the interaction Hamiltonian:

$$H_I(t) = -\frac{1}{c} \int [\mathbf{j}_e(\mathbf{r}) + \mathbf{j}_n(\mathbf{r})] \cdot \mathbf{A}(\mathbf{r}, t) d\tau, \quad (16)$$

where  $\mathbf{A}(\mathbf{r}, t)$  is the vector potential of the laser field, as described below. To solve the TDSE, we expand  $|\Psi(t)\rangle$  on the eigenstates of  $H_0$ :

$$|\Psi(t)\rangle = \sum_n C_n(t) e^{-i\omega_n t} |\psi_n\rangle, \quad (17)$$

where  $\hbar\omega_n$  is the energy of state  $|\psi_n\rangle$ . Left multiplying both sides by  $\langle\psi_m|$ , we obtain a coupled set of ordinary differential equations for the coefficients:

$$i\hbar \dot{C}_m(t) = \sum_n H_1^{mn}(t) e^{i\omega_{mn} t} C_n(t), \quad (18)$$

where  $H_1^{mn}(t) = \langle\psi_m| H_I(t) |\psi_n\rangle$  and  $\omega_{mn} = \omega_m - \omega_n$ . By solving Eq. (18), the population of each state  $|C_n(t)|^2$  at every time step can be obtained, from which the nuclear excitation probability (the population of nuclear excited states) can be determined.

The vector potential of the laser field is expressed as

$$\mathbf{A}(\mathbf{r}, t) = \frac{A_0}{2} \boldsymbol{\epsilon} f_A(t) e^{i(\mathbf{k}\cdot\mathbf{r} - \omega t)} + \text{c.c.}, \quad (19)$$

where  $\boldsymbol{\epsilon}$  is the polarization vector, and  $\mathbf{k}$  and  $\omega$  are the wave vector and angular frequency.  $A_0$  and  $f_A(t)$  are the amplitude and envelope function of the vector potential. In this article, we use  $f_A(t) = \sin^2(\pi t/T)$ , where  $T$  is the total duration of the laser field.

The plane wave term can be expanded in multipole series [50]:

$$\hat{e}_\nu e^{i\mathbf{k}\cdot\mathbf{r}} = -\nu\sqrt{2\pi} \sum_{\lambda\mu} \sqrt{2\lambda+1} i^\lambda D_{\mu\nu}^\lambda(\phi, \theta, 0) \times [A_{\lambda\mu}(\mathbf{k}; \mathbf{r}, M) + i\nu A_{\lambda\mu}(\mathbf{k}; \mathbf{r}, E)], \quad (20)$$

where  $\hat{e}_\nu$  is a spherical vector with  $\hat{e}_0 = \hat{z}$ ,  $\hat{e}_{\pm 1} = \mp \frac{1}{\sqrt{2}}(\hat{x} \pm i\hat{y})$ .  $D_{\mu\nu}^\lambda(\phi, \theta, 0)$  denotes the Wigner-D function and  $(\theta, \phi)$  describe the direction of the wave vector  $\mathbf{k}$ .  $A_{\lambda\mu}(\mathbf{k}; \mathbf{r}, \tau)$  are transverse vector spherical harmonics:

$$A_{\lambda\mu}(\mathbf{k}; \mathbf{r}, M) = \frac{1}{\hbar\sqrt{\lambda(\lambda+1)}} L[j_\lambda(kr)Y_{\lambda\mu}(\hat{r})], \quad (21)$$

$$A_{\lambda\mu}(\mathbf{k}; \mathbf{r}, E) = \frac{-i}{\hbar k\sqrt{\lambda(\lambda+1)}} \nabla \times L[j_\lambda(kr)Y_{\lambda\mu}(\hat{r})]. \quad (22)$$

For the long-wavelength limit  $kr \ll 1$ , the term  $j_\lambda(kr)$  can be approximated as  $(kr)^\lambda / (2\lambda+1)!!$ . With Eqs. (19)–(22), for a laser field, linearly polarized along the  $\hat{x}$  axis and propagating along the  $\hat{z}$  axis, the interaction matrix element can be written as

$$H_1^{mn}(t) = E_1^{mn} \mathcal{F}(t), \quad (23)$$

where  $\mathcal{F}(t) = f_A(t) \cos \omega t$ .  $E_1^{mn}$  is defined as a time-independent interaction energy between states  $m$  and  $n$ . For  $^{229}\text{Th}^{89+}$ , we denote  $E_1^{mn}$  as  $E_{\text{NHM}}^{mn}$ :

$$E_{\text{NHM}}^{mn} = 2\mathcal{E}_0 \sqrt{\frac{\pi(2F_n+1)}{6(2F_m+1)}} \sum_{\nu=\pm 1} C_{F_n m_n 1 \nu}^{F_m m_m} \mathcal{M}(M1; \overline{F}_n \rightarrow \overline{F}_m). \quad (24)$$

For the bare nucleus,  $H_0 = H_n$  and the electronic current density is zero. We denote  $E_1^{mn}$  as  $E_b^{mn}$ , which can be derived similarly:

$$E_b^{mn} = 2\mathcal{E}_0 \sqrt{\frac{\pi(2I_n+1)}{6(2I_m+1)}} \sum_{\nu=\pm 1} C_{I_n m_n 1 \nu}^{I_m m_m} \sqrt{B(M1; I_n \rightarrow I_m)}. \quad (25)$$

In both cases of  $^{229}\text{Th}^{89+}$  and  $^{229}\text{Th}^{90+}$ , the electric quadrupole ( $E2$ ) terms can be neglected due to dominance of the magnetic dipole ( $M1$ ) terms. With the interaction matrix elements, one can also calculate the transition probability using time-dependent perturbation theory (PT):

$$P_{mn}(t) = |E_1^{mn}|^2 \left| \int_{t_0}^t dt' \mathcal{F}(t') e^{i\omega_{mn} t'} \right|^2, \quad (26)$$

where the time integral is taken over the duration of the laser pulse.

### III. NUMERICAL RESULTS AND DISCUSSIONS

In this section, we present numerical results for nuclear excitation in both the bare nucleus  $^{229}\text{Th}^{90+}$  and the hydrogenlike ion  $^{229}\text{Th}^{89+}$ . We show that, as the laser intensity increases, perturbation theory breaks down and a highly nonlinear light-nucleus interaction emerges. This transition to the nonlinear regime occurs at much lower laser intensities for  $^{229}\text{Th}^{89+}$  compared to  $^{229}\text{Th}^{90+}$ . Additionally, we explore

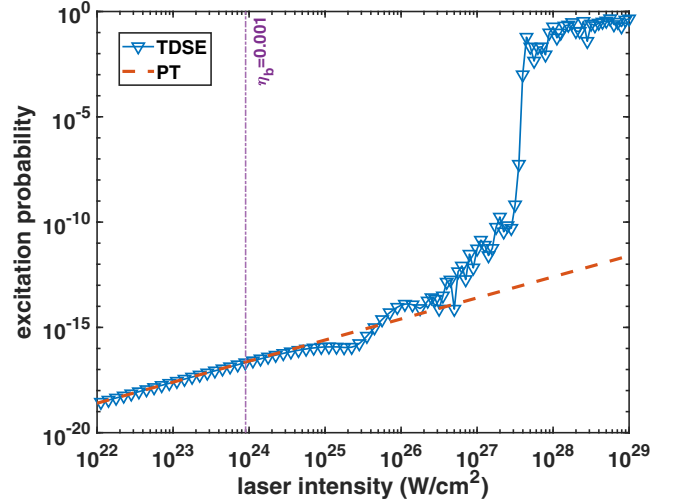


FIG. 2. Triangles: isomeric excitation probability of the bare nucleus  $^{229}\text{Th}^{90+}$  calculated by TDSE. Dashed line: excitation probability calculated by perturbation theory. The parameter  $\eta_b$  quantifies the interaction strength (see text for details), as indicated by the vertical dashed line.

how the presence of the  $1s$  electron in  $^{229}\text{Th}^{89+}$  enhances the interaction strength, enabling near-unity nuclear excitation probabilities with currently available intense lasers.

#### A. Nuclear excitation of the bare nucleus

Figure 2 shows the isomeric excitation probability of a bare nucleus at the end of the laser pulse as a function of the laser peak intensity. The laser wavelength is  $\lambda_0 = 1053$  nm. The intensity FWHM is set to 100 fs, corresponding to a total (zero-to-zero) pulse duration of approximately 283 fs.

Across the range of laser intensities, the PT results show a linear dependence, while the TDSE results can be categorized into three regions: the linear region, which closely follows PT; the surge region, characterized by a steep increase; and the saturation region, where the excitation probability maintains at high values. From  $10^{22}$  to  $10^{24}$   $\text{W}/\text{cm}^2$ , the laser intensity increases by two orders of magnitude, and the excitation probability similarly increases by two orders of magnitude. In this region, PT closely matches the TDSE results. However, from  $10^{24}$  to  $10^{26}$   $\text{W}/\text{cm}^2$ , deviations appear, indicating the breakdown of PT and the onset of nonlinear effects. In this range, PT either overestimates or underestimates the excitation probability. For laser intensities above  $10^{26}$   $\text{W}/\text{cm}^2$ , nonlinear effects dominate, and the excitation probability increases much more rapidly than in the linear regime. A two-order-of-magnitude increase in intensity (from  $10^{26}$  to  $10^{28}$   $\text{W}/\text{cm}^2$ ) results in a 14-order-of-magnitude increase in excitation probability, reaching 10%–100%. In this nonlinear regime, nuclear excitation is significantly enhanced, and PT no longer provides accurate predictions.

Figure 3 shows the time-dependent population of the nuclear isomeric state during the laser pulse at different laser intensities. At laser intensities of  $10^{24}$  and  $10^{26}$   $\text{W}/\text{cm}^2$ , the population peaks at the midpoint of the pulse, when the

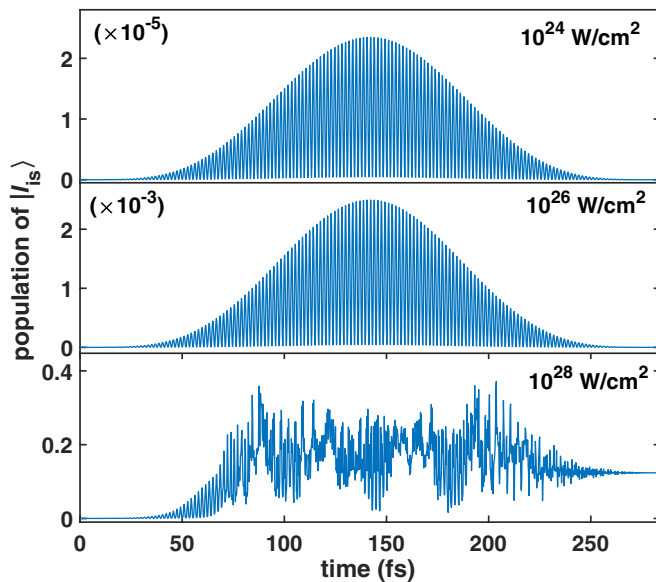


FIG. 3. Time evolution of the isomeric state population during the laser pulse for the bare nucleus  $^{229}\text{Th}^{90+}$ , calculated by TDSE at three different laser intensities.

laser field is strongest. However, the population subsequently decreases to a small value by the end of the pulse (Fig. 2 shows the end-of-pulse excitation probability). In the highly nonlinear regime, at  $10^{28} \text{ W/cm}^2$ , the nuclear states are significantly perturbed, and the final excitation probability remains significant, approximately 10%.

### B. Nuclear excitation of $^{229}\text{Th}^{89+}$

Figure 4 shows the excitation probabilities of the  $|F_3\rangle$  and  $|F_4\rangle$  states, calculated using TDSE, as a function of laser peak

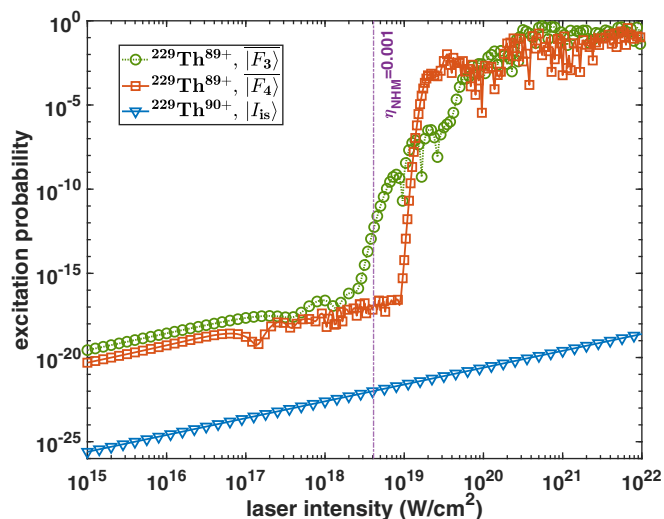


FIG. 4. Circles: Excitation probability of the  $|F_3\rangle$  state at the end of laser pulse. Squares: Excitation probability of the  $|F_4\rangle$  state at the end of laser pulse. Triangles: Excitation probability of  $^{229}\text{Th}^{90+}$  from  $|I_{gs}\rangle$  to  $|I_{is}\rangle$ .  $\eta_{\text{NHM}}$  quantifies the interaction strength of  $^{229}\text{Th}^{89+}$ , as indicated by the vertical dashed line.

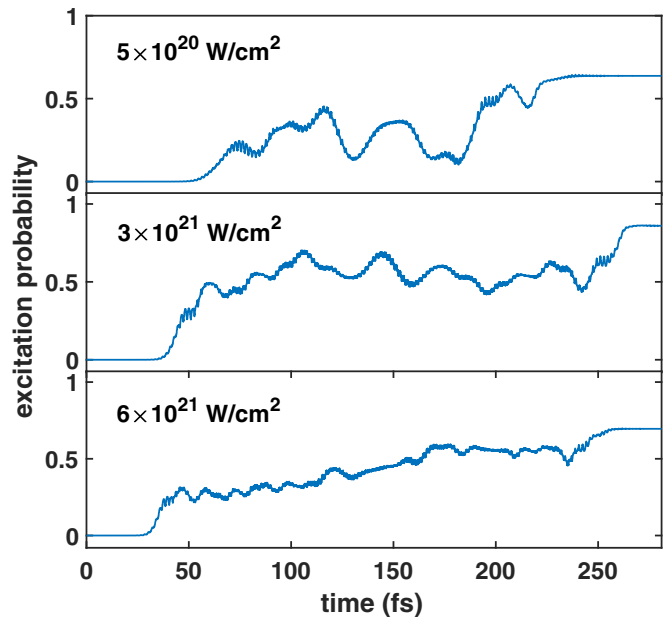


FIG. 5. Time evolution of the total isomeric excitation probability for  $^{229}\text{Th}^{89+}$  at three different laser intensities, as indicated.

intensity. The laser pulse duration and wavelength are the same as those in Fig. 2. For intensities below  $10^{17} \text{ W/cm}^2$ , the excitation probabilities for both  $^{229}\text{Th}^{90+}$  and  $^{229}\text{Th}^{89+}$  follow linear, perturbative dependencies on intensity, with the excitation probability for  $^{229}\text{Th}^{89+}$  being approximately five orders of magnitude higher than that of  $^{229}\text{Th}^{90+}$ , consistent with the difference in the  $\gamma$  decay rates.

As in the case of the bare nucleus, the excitation probabilities can be categorized into three intensity regions: the linear region, the surge region, and the saturation region. Compared to the bare-nucleus case, the surge region appears at much lower intensities, beginning between  $10^{18}$  and  $10^{19} \text{ W/cm}^2$ .

For the  $|F_3\rangle$  state, a three-order-of-magnitude increase in intensity from  $10^{18}$  to  $10^{21} \text{ W/cm}^2$  results in a 17-order-of-magnitude surge in excitation probability, from  $10^{-17}$  to nearly  $10^0$ . For the  $|F_4\rangle$  state, a two-order-of-magnitude increase in intensity from  $10^{19}$  to  $10^{21} \text{ W/cm}^2$  leads to a 16-order-of-magnitude surge, from  $10^{-17}$  to  $10^{-1}$ . The excitation probability approaches unity at intensities around  $3 \times 10^{20} \text{ W/cm}^2$ .

For  $^{229}\text{Th}^{89+}$ , the total nuclear excitation probability is the sum of the probabilities for the  $|F_3\rangle$  and  $|F_4\rangle$  states. Figure 5 shows the time evolution of the total isomeric excitation probability at three different laser intensities. At a laser intensity of  $5 \times 10^{20} \text{ W/cm}^2$ , the excitation probability at the end of the pulse is approximately 60%. At  $3 \times 10^{21} \text{ W/cm}^2$ , the end-of-pulse excitation probability increases to around 90%. At  $6 \times 10^{21} \text{ W/cm}^2$ , the excitation probability at the end of the pulse is approximately 70%.

### C. The interaction strength

To describe the onset of nonlinear effects more quantitatively, we introduce a dimensionless parameter,  $\eta$ , that

indicates the light-nucleus interaction strength:

$$\eta = \frac{E_1^{mn}}{\Delta E^{mn}}, \quad (27)$$

where the interaction energy  $E_1^{mn}$  is defined in Eqs. (23)–(25), and  $\Delta E^{mn} > 0$  is the transition energy between the two states  $|\psi_m\rangle$  and  $|\psi_n\rangle$ . Thus,  $\eta$  represents the ratio of the light-nucleus interaction energy to the nuclear transition energy. We use  $\eta_b$  for the bare nucleus case and  $\eta_{\text{NHM}}$  for the case including the NHM effect.

The vertical line in Fig. 2 marks the laser intensity where  $\eta_b = 0.001$ , averaged over all  $m_I$  substate transition channels. The corresponding laser intensity is  $9 \times 10^{23}$  W/cm<sup>2</sup>, above which the PT begins to lose validity. The vertical line in Fig. 4 marks the laser intensity where  $\eta_{\text{NHM}} = 0.001$  for the transition between  $|\overline{F}_1\rangle$  and  $|\overline{F}_3\rangle$  in  $^{229}\text{Th}^{89+}$ . The corresponding laser intensity is  $4 \times 10^{18}$  W/cm<sup>2</sup>, which is five orders of magnitude lower than in the bare-nucleus case. In other words, the presence of the  $1s$  electron reduces the laser intensity needed to induce highly nonlinear responses by five orders of magnitude.

Next, we express the magnetic dipole transition moment between  $|\overline{F}_1\rangle$  and  $|\overline{F}_3\rangle$  as

$$\begin{aligned} \mathcal{M}(M1; \overline{F}_1 \rightarrow \overline{F}_3) &= (1 - 2b^2) \sqrt{\frac{B(M1; I_{1s} \rightarrow I_{gs})}{15}} \\ &+ b\sqrt{1 - b^2} \left( \frac{5}{2\sqrt{2\pi}} \mu_e - \frac{7}{5\sqrt{2\pi}} \mu_{I_{gs}} + \frac{3}{2\sqrt{2\pi}} \mu_{I_{1s}} \right). \end{aligned} \quad (28)$$

In atomic units, the approximate values are  $\sqrt{B} \sim 10^{-7}$ ,  $\mu_{I_{gs}} \sim 10^{-6}$ ,  $\mu_{I_{1s}} \sim 10^{-6}$ , and  $\mu_e \sim 10^{-2}$ . Because  $|b| = 0.031 \ll 1$ , the dominant term is  $b\mu_e$ , which is on the order of  $10^{-4}$  a.u. This term arises from the  $1s$  electron. In contrast, the remaining purely nuclear terms, including  $\sqrt{B}$ ,  $b\mu_{I_{gs}}$ , and  $b\mu_{I_{1s}}$ , are on the order of  $10^{-7}$  or  $10^{-8}$  a.u. The interaction energy can be approximated as

$$E_1^{\text{NHM}} \approx \mathcal{E}_0 b \mu_e, \quad E_1^b \approx \mathcal{E}_0 \sqrt{B}, \quad (29)$$

where  $\mathcal{E}_0$  is the laser field amplitude. Under the same laser intensity,  $E_1^{\text{NHM}}$  is about three orders of magnitude larger than  $E_1^b$ . Since the transition energies in both systems are similar, to achieve the same  $\eta$  value, the laser field amplitude  $\mathcal{E}_0$  must be about three orders of magnitude larger for the bare nucleus, or the laser intensity must be five to six orders of magnitude greater. This accounts for the intensity difference needed in the two systems to get the same  $\eta$  value of 0.001.

It is important to note that  $\eta = 0.001$  serves as a rough indicator, rather than a precise threshold, for the emergence of nonlinear responses and the breakdown of the PT [54–60]. For  $^{229}\text{Th}^{90+}$ , nonlinear effects begin to manifest when  $\eta_b = 0.001$ , while for  $^{229}\text{Th}^{89+}$ , these effects appear even before reaching  $\eta_{\text{NHM}} = 0.001$ . Nevertheless,  $\eta$  remains a useful and intuitive parameter for making semiquantitative estimates.

## IV. FURTHER REMARKS

### A. Nonresonant excitation

The laser wavelength of 1053 nm (infrared) used in this study corresponds to Nd-doped intense laser systems. The corresponding photon energy is 1.17 eV, which does not resonate with any specific level transition in either  $^{229}\text{Th}^{90+}$  or  $^{229}\text{Th}^{89+}$ . From the energy level diagrams in Fig. 1, it is evident that the photon energy is higher than the hyperfine level splittings (which are approximately 0.7 to 0.8 eV) but much smaller than the 8.4-eV energy gap between the two nuclear levels. Consequently, the excitation scheme explored here differs significantly from typical resonant excitation schemes. This scheme leverages the high intensity of the laser field to initiate highly nonlinear responses in the target.

### B. Reliability of the numerical results

In the highly nonlinear interaction regime, the behavior of the driven system is often complex and lacks simple, intuitive explanations. For instance, the time evolution of the population in the nuclear excited state, as shown in Figs. 3 and 5, exhibits intricate dynamics. Similarly, the nuclear excitation probabilities in the saturation region, shown in Figs. 2 and 4, also fluctuate. These fluctuations are not due to numerical errors or uncertainties. In fact, the reliability and convergence of the numerical results are well assured, as the size of the Hilbert space is relatively small (10 states for the bare nucleus case and 20 states for  $^{229}\text{Th}^{89+}$ , including degenerate states with different magnetic quantum numbers), and the computational load is moderate. The observed fluctuations and complexities arise from the fundamental nature of intense light-matter interactions. Even for a two-level system interacting with light, the dynamics can become intricate when the interaction is strong and the detuning is large enough that the rotating wave approximation no longer holds [61–64].

While the fine details of the numerical results may be difficult to predict, the general trends are highly reliable and exhibit minimal sensitivity to variations in laser parameters. For example, Fig. 6(a) shows the excitation probability of the  $|\overline{F}_3\rangle$  state for different laser pulse durations. Although the specific details vary, the overarching trends remain consistent, including the onset of the surge region and the subsequent saturation region.

In our previous Letter, we employed 800-nm lasers, typical of Ti:sapphire laser systems [37]. In the current article, we deliberately use 1053-nm lasers, characteristic of Nd-doped laser systems. The pulse duration for the former laser is typically on the order of 10 fs, while for the latter it is on the order of 100 fs. This difference in pulse duration is also considered in our calculations. Despite this variation, we find that the nonlinear responses for the two intense laser sources are overall very similar.

The  $^{229}\text{Th}^{89+}$  ion is highly stable against intense laser fields. The energy gap between the  $1s_{1/2}$  state and the nearest allowed electric dipole transition, the  $2p_{1/2}$  state, is approximately 93 keV. Figure 6(b) shows the time-dependent population of the  $2p_{1/2}$  state under a laser pulse with a peak intensity of  $10^{22}$  W/cm<sup>2</sup>. (The NHM effect holds little

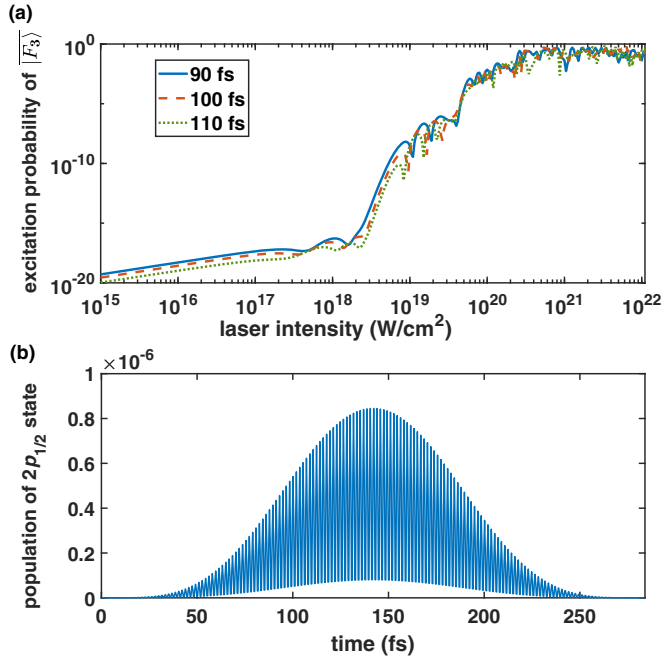


FIG. 6. (a) Excitation probability of the  $|F_3\rangle$  state for different laser durations as a function of laser intensity. (b) Time evolution of the electronic  $2p_{1/2}$  state population under a laser intensity of  $10^{22}$  W/cm $^2$ .

significance as it does not influence the electric dipole transition in this case). The excitation probability to this state is on the order of  $10^{-6}$  during the laser pulse, but drops to a much lower value at the end of the pulse. Excitation to other electronic states is even less probable.

### C. Potential experiment

The results presented in this article highlight the potential for manipulating single-nucleus states, which could be experimentally validated using various existing facilities. Hydrogenlike highly charged ions (HCIs) can be generated and stored in ion storage rings [65–67] or electron beam ion traps (EBIT) [68–70]. Penning traps, as auxiliary equipment, offer the capability to cool and confine single ions or ion bunches for extended periods, exceeding 1 s [71,72]. These facilities can be integrated with superintense lasers to enable advanced research [71–74]. Below, we outline potential experimental scenarios:

(i) Laser intensities above  $10^{20}$  W/cm $^2$  are achievable with petawatt (PW) lasers. For instance, a 1 PW laser focused to a beam waist of  $w_0 = 15$   $\mu\text{m}$  produces a focal depth of  $d = 2\pi w_0^2/\lambda_0 = 1.3$  mm and a peak intensity of  $4.4 \times 10^{20}$  W/cm $^2$ . A 10 PW laser focused to  $w_0 = 30$   $\mu\text{m}$  results in a focus depth of 5 mm and a peak intensity of  $10^{21}$  W/cm $^2$ . These sizes are compatible with Penning traps such as HILITE and ALPHATRAP, which can confine  $10^3$  to  $10^7$   $^{229}\text{Th}^{89+}$  ions at low temperatures (around 4 K) [71,72]. Moreover, HILITE is a mobile trap, enabling integration with an EBIT that generates HCIs and a strong laser for comprehensive experiments [72].

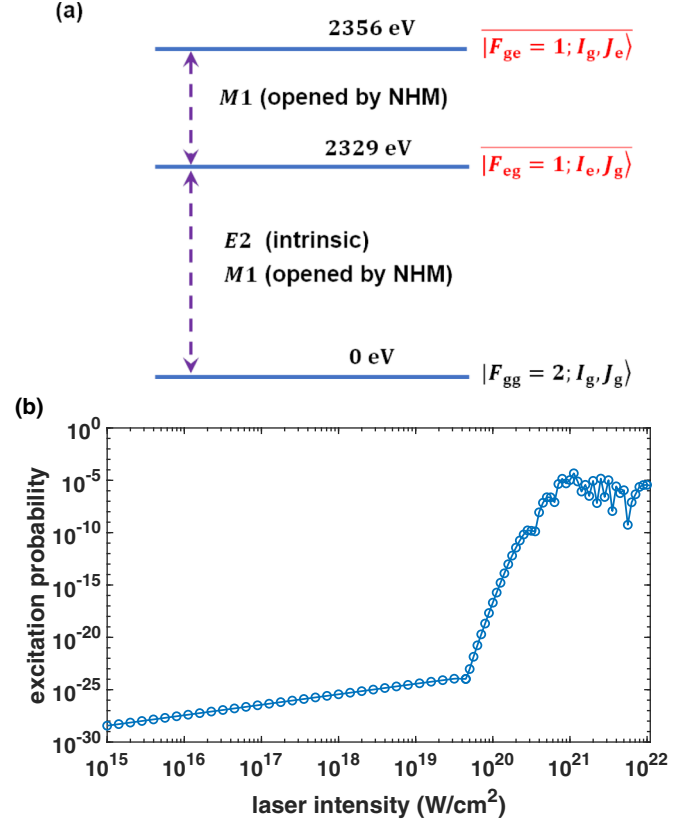


FIG. 7. (a) Energy-level structure of  $^{205}\text{Pb}^{77+}$ .  $I$  represents the spin of the nucleus and  $J$  is the angular momentum of the valence electron. The energy levels are not drawn to scale. (b) End-of-pulse excitation probability of  $^{205}\text{Pb}^{77+}$  from  $|F_{eg} = 1\rangle$  to  $|F_{ge} = 1\rangle$  as a function of laser intensity. The laser is assumed to be linearly polarized with a wavelength of 1053 nm and a pulse duration of 100 fs (FWHM in intensity).

(ii) Ion storage rings also provide excellent experimental platforms. For example, ESR in Germany and CSRe in China can generate low-energy HCI bunches containing up to  $10^8$  ions [65,66]. Notably, the HIAF facility in China, currently under construction, aims to achieve up to  $10^{11}$  ions per bunch [67]. These ion bunches can interact with superintense lasers at experimental stations within the accelerator. Systems like PHELIX (Petawatt High-Energy Laser for Heavy-Ion Experiments), integrated with ESR's ion beams, combine high-energy laser pulses and heavy-ion beams [75–77]. PHELIX generates strong lasers at 1053 nm, with intensities ranging from  $10^{20}$  to  $10^{21}$  W/cm $^2$  and durations on the order of 100 fs.

### D. Excitation of $^{205}\text{Pb}^{77+}$

The highly nonlinear effect presented above for  $^{229}\text{Th}$  can also be expected in other systems, such as boronlike  $^{205}\text{Pb}$  ( $^{205}\text{Pb}^{77+}$ ), which also exhibits substantial NHM [78]. The nuclear ground and isomeric states of  $^{205}\text{Pb}$  have spin-parity values  $I_g^\pi = 5/2^-$  and  $I_e^\pi = 1/2^-$ , respectively, with the isomeric state located 2329 eV above the ground state. In the

boronlike charge state, a valence  $2p_{1/2}$  electron ( $J_g = 1/2$ ) is present, and the first electronic excited state  $2p_{3/2}$  ( $J_e = 3/2$ ) lies 2356 eV above. Figure 7(a) shows a partial energy-level structure of  $^{205}\text{Pb}^{77+}$ . For simplicity, the hyperfine splittings (on the order of  $10^{-2}$  eV) of each level are not shown. Due to the proximity of the nuclear isomeric and electronic excited states, the energy difference between the nucleus-electron coupled states  $|F_{eg}\rangle$  and  $|F_{ge}\rangle$  is only 27 eV. This leads to a significant NHM effect between the two states with the same total angular momentum  $F = 1$ . The calculated mixing coefficient is  $b' = -1.97 \times 10^{-5}$ . It was found that the inclusion of NHM opens a new  $M1$  transition, dramatically reducing the nuclear radiative half-life from 15 min to 32 ms [78].

Figure 7(b) presents the end-of-pulse excitation probability from  $|F_{eg} = 1\rangle$  to  $|F_{ge} = 1\rangle$  under a linearly polarized laser with a wavelength of 1053 nm and a pulse duration of 100 fs. This calculation is also performed using the TDSE described above. It can be seen that the highly nonlinear excitation also appears in this case, which can be categorized into similar three regions. In the surge region, where the laser intensity increases from  $10^{20}$  to  $10^{21}$  W/cm<sup>2</sup>, the excitation probability rises by 20 orders of magnitude. In this case, the excitation probability saturates around  $10^{-5}$ . This limitation arises from the small mixing coefficient and the intrinsic magnetic dipole moment of the system.  $^{205}\text{Pb}^{77+}$  is stable under the laser intensity presented in Fig. 7(b). The energy gap between the  $2p_{1/2}$  state and the nearest allowed electric-dipole destination, the  $3s_{1/2}$  state, is about 13.6 keV. The excitation probability to this state during the pulse is only on the order of  $10^{-5}$  under an intensity of  $10^{22}$  W/cm<sup>2</sup>.

## V. CONCLUSION

Through a detailed investigation of the NHM effect and the interaction between an intense laser pulse and the  $^{229}\text{Th}$  nucleus, we have conducted an in-depth analysis of the nuclear excitation phenomenon in both the bare nucleus and the hydrogenlike ion. Our study explores the highly nonlinear nature of the excitation process, yielding several notable findings. Specifically, we have demonstrated highly efficient nuclear isomeric excitation within this nonlinear light-nucleus interaction regime. Our analysis underscores the critical role of the NHM-enhanced transition moment, thereby lowering the intensity requirements compared to the bare nucleus. Notably, we show that such remarkable excitation efficiency can be consistently achieved across a broad range of laser parameters.

The high excitation efficiency achieved in our study has profound implications for manipulating atomic nuclei with light. It paves the way for quantum state control of individual nuclei or collective excitation within an ion bunch. The results of our work can be readily implemented in existing experimental setups, highlighting their practical significance and immediate applicability.

## ACKNOWLEDGMENT

This work was supported by NSFC Grants No. 12474484, No. U2330401, and No. 12088101.

## DATA AVAILABILITY

The data that support the findings of this article are openly available [79].

- 
- [1] E. Peik and Chr. Tamm, Nuclear laser spectroscopy of the 3.5 eV transition in Th-229, *Europhys. Lett.* **61**, 181 (2003).
  - [2] J. Tiedau, M. V. Okhapkin, K. Zhang, J. Thielking, G. Zitzer, E. Peik, F. Schaden, T. Pronebner, I. Morawetz, L. Toscani De Col *et al.*, Laser excitation of the Th-229 nucleus, *Phys. Rev. Lett.* **132**, 182501 (2024).
  - [3] R. Elwell, C. Schneider, J. Jeet, J. E. S. Terhune, H. W. T. Morgan, A. N. Alexandrova, H. B. Tran Tan, A. Derevianko, and E. R. Hudson, Laser excitation of the  $^{229}\text{Th}$  nuclear isomeric transition in a solid-state host, *Phys. Rev. Lett.* **133**, 013201 (2024).
  - [4] C. Zhang, T. Ooi, J. S. Higgins, J. F. Doyle, L. von der Wense, K. Beeks, A. Leitner, G. Kazakov, P. Li, P. G. Thirolf *et al.*, Frequency ratio of the  $^{229\text{m}}\text{Th}$  nuclear isomeric transition and the  $^{87}\text{Sr}$  atomic clock, *Nature (London)* **633**, 63 (2024).
  - [5] G. C. Baldwin and J. C. Solem, Recoilless gamma-ray lasers, *Rev. Mod. Phys.* **69**, 1085 (1997).
  - [6] E. V. Tkalya, Proposal for a nuclear gamma-ray laser of optical range, *Phys. Rev. Lett.* **106**, 162501 (2011).
  - [7] E. V. Tkalya and L. P. Yatsenko, Creation of inverse population in the  $^{229}\text{Th}$  ground state doublet by means of a narrowband laser, *Laser Phys. Lett.* **10**, 105808 (2013).
  - [8] P. Walker and G. Dracoulis, Energy traps in atomic nuclei, *Nature (London)* **399**, 35 (1999).
  - [9] J. J. Carroll, S. Karamian, L. A. Rivlin, and A. A. Zernovskiy, X-ray-driven gamma emission, *Hyperfine Interact.* **135**, 3 (2001).
  - [10] T. Masuda, A. Yoshimi, A. Fujieda, H. Fujimoto, H. Haba, H. Hara, T. Hiraki, H. Kaino, Y. Kasamatsu, S. Kitao *et al.*, X-ray pumping of the  $^{229}\text{Th}$  nuclear clock isomer, *Nature (London)* **573**, 238 (2019).
  - [11] T. Hiraki, K. Okai, M. Bartokos, K. Beeks, H. Fujimoto, Y. Fukunaga, H. Haba, Y. Kasamatsu, S. Kitao, A. Leitner *et al.*, Controlling  $^{229}\text{Th}$  isomeric state population in a VUV transparent crystal, *Nat. Commun.* **15**, 5536 (2024).
  - [12] Y. Shvyd'ko, R. Röhlsberger, O. Kocharovskaya, J. Evers, G. A. Geloni, P. Liu, D. Shu, A. Miceli, B. Stone, W. Hippler *et al.*, Resonant X-ray excitation of the nuclear clock isomer  $^{45}\text{Sc}$ , *Nature (London)* **622**, 471 (2023).
  - [13] J. Haber, X. Kong, C. Strohm, S. Willing, J. Gollwitzer, I. Bocklage, R. Ruffer, A. Pálffy, and R. Röhlsberger, Rabi oscillations of x-ray radiation between two nuclear ensembles, *Nat. Photon.* **11**, 720 (2017).
  - [14] K. P. Heeg, A. Kaldun, C. Strohm, C. Ott, R. Subramanian, D. Lentrodt, J. Haber, H.-C. Wille, S. Goerttler, R. Ruffer *et al.*, Coherent x-ray-optical control of nuclear excitons, *Nature (London)* **590**, 401 (2021).

- [15] T. J. Bürvenich, J. Evers, and C. H. Keitel, Nuclear quantum optics with X-ray laser pulses, *Phys. Rev. Lett.* **96**, 142501 (2006).
- [16] T. J. Bürvenich, J. Evers, and C. H. Keitel, Dynamic nuclear Stark shift in superintense laser fields, *Phys. Rev. C* **74**, 044601 (2006).
- [17] K. Alder, A. Bohr, T. Huus, B. Mottelson, and A. Winther, Study of nuclear structure by electromagnetic excitation with accelerated ions, *Rev. Mod. Phys.* **28**, 432 (1956).
- [18] T. Glasmacher, Intermediate-energy Coulomb excitation, *Nucl. Phys. A* **693**, 90 (2001).
- [19] A. Görge and W. Korten, Coulomb excitation studies of shape coexistence in atomic nuclei, *J. Phys. G* **43**, 024002 (2016).
- [20] T. Li, H. Zhang, and X. Wang, Theory of Coulomb excitation of the  $^{229}\text{Th}$  nucleus by protons, *Phys. Rev. C* **108**, L041602 (2023).
- [21] E. V. Tkalya, Probability of nonradiative excitation of nuclei in transitions of an electron in an atomic shell, *Zh. Eksp. Teor. Fiz.* **102**, 379 (1992) [*Sov. Phys. JETP* **75**, 200 (1992)].
- [22] E. V. Tkalya, Excitation of  $^{229\text{m}}\text{Th}$  at inelastic scattering of low energy electrons, *Phys. Rev. Lett.* **124**, 242501 (2020).
- [23] H. Zhang, W. Wang, and X. Wang, Nuclear excitation cross section of  $^{229}\text{Th}$  via inelastic electron scattering, *Phys. Rev. C* **106**, 044604 (2022).
- [24] B. Liu and X. Wang, Isomeric excitation of  $^{235}\text{U}$  by inelastic scattering of low-energy electrons, *Phys. Rev. C* **106**, 064604 (2022).
- [25] S. G. Porsev, V. V. Flambaum, E. Peik, and C. Tamm, Excitation of the isomeric  $^{229\text{m}}\text{Th}$  nuclear state via an electronic bridge process in  $^{229}\text{Th}^+$ , *Phys. Rev. Lett.* **105**, 182501 (2010).
- [26] R. A. Müller, A. V. Volotka, and A. Surzhykov, Excitation of the  $^{229}\text{Th}$  nucleus via a two-photon electronic transition, *Phys. Rev. A* **99**, 042517 (2019).
- [27] A. Ya. Dzyublik, Excitation of  $^{229\text{m}}\text{Th}$  in the electron bridge via continuum as a scattering process, *Phys. Rev. C* **102**, 024604 (2020).
- [28] W. Wang, J. Zhou, B. Liu, and X. Wang, Exciting the isomeric  $^{229}\text{Th}$  nuclear state via laser-driven electron recollision, *Phys. Rev. Lett.* **127**, 052501 (2021).
- [29] X. Wang, Nuclear excitation of  $^{229}\text{Th}$  induced by laser-driven electron recollision, *Phys. Rev. C* **106**, 024606 (2022).
- [30] J. Feng, W. Wang, C. Fu, L. Chen, J. Tan, Y. Li, J. Wang, Y. Li, G. Zhang, Y. Ma, and J. Zhang, Femtosecond pumping of nuclear isomeric states by the coulomb collision of ions with quivering electrons, *Phys. Rev. Lett.* **128**, 052501 (2022).
- [31] J. Qi, H. Zhang, and X. Wang, Isomeric excitation of  $^{229}\text{Th}$  in laser-heated clusters, *Phys. Rev. Lett.* **130**, 112501 (2023).
- [32] J. Feng, J. Qi, H. Zhang, S. Chen, M. Zhu, X. Hu, H. Xu, C. Fu, X. Wang, L. Chen, and J. Zhang, Laser-based approach to measure small nuclear cross sections in plasma, *Proc. Natl. Acad. Sci. USA* **121**, e2413221121 (2024).
- [33] P. Agostini, F. Fabre, G. Mainfray, G. Petite, and N. K. Rahman, Free-free transitions following six-photon ionization of xenon atoms, *Phys. Rev. Lett.* **42**, 1127 (1979).
- [34] D. N. Fittinghoff, P. R. Bolton, B. Chang, and K. C. Kulander, Observation of nonsequential double ionization of helium with optical tunneling, *Phys. Rev. Lett.* **69**, 2642 (1992).
- [35] W. Becker, X. J. Liu, P. J. Ho, and J. H. Eberly, Theories of photoelectron correlation in laser-driven multiple atomic ionization, *Rev. Mod. Phys.* **84**, 1011 (2012).
- [36] S. Laroche, A. Talebpour, and S. L. Chin, Non-sequential multiple ionization of rare gas atoms in a Ti: Sapphire laser field, *J. Phys. B: At. Mol. Opt. Phys.* **31**, 1201 (1998).
- [37] H. Zhang, T. Li, and X. Wang, Highly nonlinear light-nucleus interaction, *Phys. Rev. Lett.* **133**, 152503 (2024).
- [38] L. A. Kroger, and C. W. Reich, Features of the low-energy level scheme of  $^{229}\text{Th}$  as observed in the  $\alpha$ -decay of  $^{233}\text{U}$ , *Nucl. Phys. A* **259**, 29 (1976).
- [39] Z. Zhang, F. Wu, J. Hu, X. Yang, J. Gui, P. Ji, X. Liu, C. Wang, Y. Liu, X. Lu *et al.*, The 1 PW/0.1 Hz laser beamline in SULF facility, *High Power Laser Sci. Eng.* **8**, e4 (2020).
- [40] J. W. Yoon, Y. G. Kim, I. W. Choi, J. H. Sung, H. W. Lee, S. K. Lee, and C. H. Nam, Realization of laser intensity over  $10^{23}\text{W}/\text{cm}^2$ , *Optica* **8**, 630 (2021).
- [41] C. Schwartz, Hyperfine Structure, *Phys. Rev.* **97**, 380 (1955).
- [42] R. D. Cowan, *The Theory of Atomic Structure and Spectra* (University of California Press, Berkeley, 1981).
- [43] A. Bohr and B. R. Mottelson, *Nuclear Structure* (World Scientific, Singapore, 1998), Vol. 1.
- [44] J. Thielking, M. V. Okhapkin, P. Glowacki, D. M. Meier, L. von der Wense, B. Seiferle, C. E. Düllmann, P. G. Thirolf, and E. Peik, Laser spectroscopic characterization of the nuclear-clock isomer  $^{229\text{m}}\text{Th}$ , *Nature (London)* **556**, 321 (2018).
- [45] M. S. Safronova, U. I. Safronova, A. G. Radnaev, C. J. Campbell, and A. Kuzmich, Magnetic dipole and electric quadrupole moments of the  $^{229}\text{Th}$  nucleus, *Phys. Rev. A* **88**, 060501(R) (2013).
- [46] S. Wycech and J. Żylicz, Predictions for nuclear spin mixing in magnetic fields, *Acta Phys. Pol. B* **24**, 637 (1993).
- [47] F. F. Karpeshin, S. Wycech, I. M. Band, M. B. Trzhaskovskaya, M. Pfützner, and J. Żylicz, Rates of transitions between the hyperfine-splitting components of the ground-state and the 3.5 eV isomer in  $^{229}\text{Th}^{89+}$ , *Phys. Rev. C* **57**, 3085 (1998).
- [48] E. V. Tkalya, and A. V. Nikolaev, Magnetic hyperfine structure of the ground-state doublet in highly charged ions  $^{229}\text{Th}^{89+.87+}$  and the Bohr-Weisskopf effect, *Phys. Rev. C* **94**, 014323 (2016).
- [49] V. M. Shabaev, D. A. Glazov, A. M. Ryzhkov, C. Brandau, G. Plunien, W. Quint, A. M. Volchkova, and D. V. Zinenko, Ground-state  $g$  factor of highly charged  $^{229}\text{Th}$  ions: An access to the M1 transition probability between the isomeric and ground nuclear states, *Phys. Rev. Lett.* **128**, 043001 (2022).
- [50] J. M. Eisenberg and W. Greiner, *Excitation Mechanisms of the Nucleus* (North-Holland, Amsterdam, 1987), Vol. 2.
- [51] N. Minkov and A. Pálffy,  $^{229\text{m}}\text{Th}$  isomer from a nuclear model perspective, *Phys. Rev. C* **103**, 014313 (2021).
- [52] A. Yamaguchi, Y. Shigekawa, H. Haba, H. Kikunaga, K. Shirasaki, M. Wada, and H. Katori, Laser spectroscopy of triply charged  $^{229}\text{Th}$  isomer for a nuclear clock, *Nature (London)* **629**, 62 (2024).
- [53] S. Kraemer, J. Moens, M. Athanasakis-Kaklamanakis, S. Bara, K. Beeks, P. Chhetri, K. Chrysalidis, A. Claessens, T. E. Cocolios, J. G. M. Correia *et al.*, Observation of the radiative decay of the  $^{229}\text{Th}$  nuclear clock isomer, *Nature (London)* **617**, 706 (2023).
- [54] A. A. Anappara, S. D. Liberato, A. Tredicucci, C. Ciuti, G. Biasiol, L. Sorba, and F. Beltram, Signatures of the ultrastrong light-matter coupling regime, *Phys. Rev. B* **79**, 201303(R) (2009).
- [55] S. Gambino, M. Mazzeo, A. Genco, O. D. Stefano, S. Savasta, S. Patané, D. Ballarini, F. Mangione, G. Lerario, D. Sanvitto *et al.*, Exploring light-matter interaction phenomena

- under ultrastrong coupling regime, *ACS Photonics* **1**, 1042 (2014).
- [56] A. Bayer, M. Pozimski, S. Schambeck, D. Schuh, R. Huber, D. Bougeard, and C. Lange, Terahertz light-matter interaction beyond unity coupling strength, *Nano Lett.* **17**, 6340 (2017).
- [57] P. Forn-Díaz, J. J. García-Ripoll, B. Peropadre, J. L. Orgiazzi, M. A. Yurtalan, R. Belyansky, C. M. Wilson, and A. Lupascu, Ultrastrong coupling of a single artificial atom to an electromagnetic continuum in the nonperturbative regime, *Nat. Phys.* **13**, 39 (2017).
- [58] A. F. Kockum, A. Miranowicz, S. D. Liberato, S. Savasta, and F. Nori, Ultrastrong coupling between light and matter, *Nat. Rev. Phys.* **1**, 19 (2019).
- [59] P. Forn-Díaz, L. Lamata, E. Rico, J. Kono, and E. Solano, Ultrastrong coupling regimes of light-matter interaction, *Rev. Mod. Phys.* **91**, 025005 (2019).
- [60] J. Koch, G. R. Hunanyan, T. Ockenfels, E. Rico, E. Solano, and M. Weitz, Quantum Rabi dynamics of trapped atoms far in the deep strong coupling regime, *Nat. Commun.* **14**, 954 (2023).
- [61] N. B. Delone, V. P. Krařnov, and V. A. Khodovoi, The two-level system in a strong light field, *Sov. Phys. Usp.* **18**, 750 (1975).
- [62] F. I. Gauthey, B. M. Garraway, and P. L. Knight, High harmonic generation and periodic level crossings, *Phys. Rev. A* **56**, 3093 (1997).
- [63] Y. Wu and X. Yang, Strong-coupling theory of periodically driven two-level systems, *Phys. Rev. Lett.* **98**, 013601 (2007).
- [64] I. D. Feranchuk and A. V. Leonov, Strong field effects in the evolution of a two-level system, *Phys. Lett. A* **375**, 385 (2011).
- [65] W. Q. Wen, M. Lochmann, X. Ma, M. Bussmann, D. F. A. Winters, W. Nörtershäuser, B. Botermann, C. Geppert, N. Frömmgen, M. Hammen *et al.*, Optical measurement of the longitudinal ion distribution of bunched ion beams in the ESR, *Nucl. Instrum. Methods Phys. Res. Sect. A* **711**, 90 (2013).
- [66] X. Ma, W. Wen, Z. Huang, H. Wang, Y. Yuan, M. Wang, Z. Sun, L. Mao, J. Yang, and H. Xu, Proposal for precision determination of 7.8 eV isomeric state in  $^{229}\text{Th}$  at heavy ion storage ring, *Phys. Scr.* **T166**, 014012 (2015).
- [67] J. Yang, J. Xia, G. Xiao, H. Xu, H. Zhao, X. Zhou, X. Ma, Y. He, L. Ma, D. Gao *et al.*, High intensity heavy ion accelerator facility (HIAF) in China, *Nucl. Instrum. Methods Phys. Res. Sect. B* **317**, 263 (2013).
- [68] R. E. Marrs, S. R. Elliott, and D. A. Knapp, Production and trapping of hydrogenlike and bare uranium ions in an electron beam ion trap, *Phys. Rev. Lett.* **72**, 4082 (1994).
- [69] A. J. G. Martínez, J. C. López-Urrutia, D. Fischer, R. Soria Orts, and J. Ullrich, The Heidelberg EBIT: Present results and future perspectives, *J. Phys.: Conf. Ser.* **72**, 012001 (2007).
- [70] P. Micke, S. Kuhn, L. Buchauer, J. Harries, T. M. Bucking, K. Blaum, A. Cieluch, A. Egl, D. Hollain, S. Kraemer *et al.*, The Heidelberg compact electron beam ion traps, *Rev. Sci. Instrum.* **89**, 063109 (2018).
- [71] S. Sturm, I. Arapoglou, A. Egl, M. Höcker, S. Kraemer, T. Sailer, B. Tu, A. Weigel, R. Wolf, J. Crespo López-Urrutia *et al.*, The ALPHATRAP experiment, *Eur. Phys. J.: Spec. Top.* **227**, 1425 (2019).
- [72] M. Vogel, W. Quint, G. G. Paulus, and Th. Stöhlker, A Penning trap for advanced studies with particles in extreme laser fields, *Nucl. Instrum. Methods Phys. Res. Sect. B* **285**, 65 (2012).
- [73] S. Bernitt, G. V. Brown, J. K. Rudolph, R. Steinbrügge, A. Graf, M. Leutenegger, S. W. Epp, S. Eberle, K. Kubiček, V. Mäckel *et al.*, An unexpectedly low oscillator strength as the origin of the Fe XVII emission problem, *Nature (London)* **492**, 225 (2012).
- [74] S. Ringleb, M. Kiffer, N. Stallkamp, S. Kumar, J. Hofbrucker, B. Reich, B. Arndt, G. Brenner, M. Ruiz-López, S. Dusterer *et al.*, High-intensity laser experiments with highly charged ions in a Penning trap, *Phys. Scr.* **97**, 084002 (2022).
- [75] Zs. Major, U. Eisenbarth, B. Zielbauer, C. Brabetz, J. B. Ohland, Y. Zobus, S. Roeder, D. Reemts, S. Kunzer, S. Götte *et al.*, High-energy laser facility PHELIX at GSI: Latest advances and extended capabilities, *High Power Laser Sci. Eng.* **12**, e39 (2024).
- [76] M. G. Kozlov, M. S. Safronova, J. R. Crespo López-urrutia, and P. O. Schmidt, Highly charged ions: Optical clocks and applications in fundamental physics, *Rev. Mod. Phys.* **90**, 045005 (2018).
- [77] M. Steck and Y. A. Litvinov, Heavy-ion storage rings and their use in precision experiments with highly charged ions, *Prog. Part. Nucl. Phys.* **115**, 103811 (2020).
- [78] W. Wang and X. Wang, Substantial nuclear hyperfine mixing effect in boronlike  $^{205}\text{Pb}$  ions, *Phys. Rev. Lett.* **133**, 032501 (2024).
- [79] H. Zhang, Highli nonlinear nuclear excitation. figshare. Figure. (2024), <https://doi.org/10.6084/m9.figshare.28106618.v1>.